Remote distribution of the quantum coherence resource through optical fiber

Juan Yu ⬤,[1] Yinhua Wu,[1] Wangyun Liu,[1] Zhihui Yan ⬤,[2,3,*] and Xiaojun Jia[2,3]

[1]*School of Optoelectronic Engineering, Xi'an Technological University, Xi'an 710021, People's Republic of China*
[2]*State Key Laboratory of Quantum Optics and Quantum Optics Devices, Institute of Opto-Electronics,*
Shanxi University, Taiyuan, 030006, People's Republic of China
[3]*Collaborative Innovation Center of Extreme Optics, Shanxi University, Taiyuan 030006, People's Republic of China*

As one of the most remarkable features of quantum mechanics, quantum coherence is regarded as an invaluable quantum resource in quantum information. Using the optical fiber as one of the effective quantum channels, the remote distribution of quantum coherence through fiber is essential for potential practical applications. Here we propose the remote distribution scheme of the quantum coherence resource through an optical fiber. The two-mode squeezed state (TMSS) generated by the nondegenerate optical parametric amplifier is distributed through optical fibers, and the quantum coherence of the TMSS is analyzed by the relative entropy of the covariance matrix. We show that quantum coherence is robust against the distribution distance even if the entanglement disappears at short distribution distance due to the loss and excess noise in fiber channels. Our results provide a direct reference for the potential practical applications of quantum coherence.

I. INTRODUCTION

The coherent superposition of states represents one of the most fundamental features that marks the departure of quantum mechanics from the classical realm, systems in such superposition states are often said to possess quantum coherence. Coherence plays an important role in quantum thermodynamics [1–3], biological systems [4,5], quantum algorithm [6], quantum metrology [7,8], and so on. The research of quantum coherence is very attractive. Quantum coherence of the quantum state is defined as the distance between the quantum state and its nearest incoherent state in the Hilbert space. The framework to quantify coherence is established by referring to the method of quantifying entanglement [9,10], and it can be quantified by relative entropy [11], the l_1 norm [9], skew information entropy [12], Fisher information [13], and so on. Recently, significant progress in quantum coherence has been theoretically and experimentally achieved [14–19]. Coherence of a tunable quantum detector has been experimentally quantified, based on a recently developed resource theory of quantum operations [20]. The basis-independent (or reference frame-independent) quantification of coherence is achieved by a set of quantum states [21]. In addition, the tracking of quantum coherence in polariton condensates with time-resolved tomography has been experimentally proved [23]. Besides the investigations of its character, quantum coherence can be applied in quantum information. By manipulating quantum coherence, the allowing correlation among multiple catalysts can offer arbitrary power [22]. The fragility of quantum coherence in the presence of decoherence and this conjecture has been experimentally confirmed [24,25] for discrete-variable (DV) systems. The quantum coherence of Gaussian states is robust against loss and noise in simulated Gaussian thermal noise channels [26,27]. Both DV and continuous-variable (CV) quantum technologies have been developed in parallel with their own advantages in quantum information science. High fidelity can be achieved with DV systems, while the CV systems possess the deterministic advantage. The tradeoff between high fidelity and deterministic technology can be solved by combining these two approaches in more powerful hybrid protocols [28].

The remote distribution of quantum resources is not only of interest in the understanding of a physical mechanism such as decoherence, but also of crucial importance for the practical applications of a quantum network [28–34]. With the help of a low-Earth orbit satellite, ground-to-satellite quantum teleportation with a single photon over 1000 kilometers has been realized [35,36]. The optical fiber is one of the effective and reliable channels for the transmission of quantum information [37–42], and its advantage is that it is low-cost and easily compatible with the present commercial communication system. In addition, the transmission distance of quantum communication over 100 kilometres in fiber has been realized [43–46]. In the optical fiber channel, the transmission loss and excess noise induced by the guided acoustic wave Brillouin scattering (GAWBS) processing have to be considered for the distribution of quantum resources. The simulation of GAWBS noise is mainly due to the fluctuation of the density of optical fibers in time and space caused by the acoustic field, which results from the continuous thermal motion of the particles in the optical medium [47]. Quantum coherence is an important quantum resource, and it is in high demand to investigate the remote distribution of quantum coherence resources for its potential practical application in quantum communication.

*zhyan@sxu.edu.cn

Here, we propose a deterministic remote distribution scheme of quantum coherence resources through optical fibers. The two-mode squeezed state (TMSS) generated by nondegenerate optical parametric amplifier (NOPA) is distributed to quantum users, and quantum coherence of the TMSS is quantified by calculating the relative entropy from the covariance matrix. The quantum coherence of TMSS depends on the various parameters of the actual experimental generation system and the main factors affecting distribution distance are the transmission loss and extra noise induced by the GAWBS in fiber channels. The influence of various parameters of NOPA on the quantum coherence and entanglement of TMSS is analyzed in detail by solving quantum Langevin motion equations. In addition, we experimentally characterize the evolution of quantum coherence and entanglement of TMSS in fiber channels. We show that the quantum coherence of TMSS is robust against the distribution distance even if the entanglement disappears at short distribution distance due to loss and excess noise in fiber channels. The remote distribution scheme of the quantum coherence resources of TMSS is experimentally feasible. Our results provide a direct reference for the experimental research and the foundation for potential practical applications of quantum coherence in quantum communication.

The paper is organized as follows. In Sec. II we quantify the quantum coherence of TMSS with NOPA and analyze the influence of various parameters of NOPA on the quantum coherence. The deterministic remote distribution scheme of the quantum coherence of TMSS through optical fibers is proposed and analyzed in Sec. III. A brief summary is provided in Sec. IV.

II. QUANTIFYING COHERENCE OF TMSS WITH NOPA

Quantum coherence of a quantum state $\hat{\rho}$ in Fock space can be calculated by [9]

$$C(\hat{\rho}) = S(\hat{\rho}_{\text{diag}}) - S(\hat{\rho}), \qquad (1)$$

where S is the von Neumann entropy and $\hat{\rho}_{\text{diag}}$ denotes the state obtained from $\hat{\rho}$ by deleting all off-diagonal elements with the mean number. A Gaussian state can be completely characterized by the displacement $\bar{\mathbf{x}}$ and the covariance matrix σ in phase space in quantum information [48], so it is natural to demand a coherence measure in terms of the covariance matrix and displacement vector. The displacement $\bar{\mathbf{x}} = \langle \mathbf{x} \rangle$, where $\mathbf{x} = (\hat{x}_1, \hat{y}_1, \ldots, \hat{x}_N, \hat{y}_N)^t$, $\hat{x} = \hat{a} + \hat{a}^\dagger$, and $\hat{y} = (\hat{a} - \hat{a}^\dagger)/i$ are the amplitude and phase quadratures of an optical field, respectively. The element of the covariance matrix is defined as $\sigma_{ij} = \text{Cov}(\mathbf{x}_i, \mathbf{x}_j) = \frac{1}{2}\langle \mathbf{x}_i \mathbf{x}_j + \mathbf{x}_j \mathbf{x}_i \rangle - \langle \mathbf{x}_i \rangle \langle \mathbf{x}_j \rangle$.

For general N-mode Gaussian states $\hat{\rho}(\bar{\mathbf{x}}, \sigma)$, the closed-form expression for the quantification of quantum coherence is as follows [14]:

$$C[\hat{\rho}(\bar{\mathbf{x}}, \sigma)] = \sum_{i=1}^{N} [(\bar{n}_i + 1) \log_2 (\bar{n}_i + 1) - \bar{n}_i \log_2 \bar{n}_i)] - S(\hat{\rho}),$$
$$(2)$$

where $S(\hat{\rho}) = \sum_{i=1}^{N}[(\frac{\nu_i+1}{2}) \log_2(\frac{\nu_i+1}{2}) - (\frac{\nu_i-1}{2}) \log_2(\frac{\nu_i-1}{2})]$, ν_i is the symplectic eigenvalue of σ, and $\bar{n}_i = 1/4[\sigma_{2i-1,2i-1} + \sigma_{2i,2i} + (\bar{\mathbf{x}}_{2i-1})^2 + (\bar{\mathbf{x}}_{2i})^2 - 2]$ is the mean number of the ith mode.
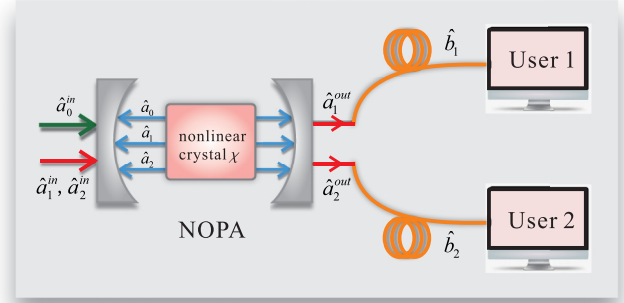
FIG. 1. Schematic of the generation and remote distribution of quantum coherence resources through optical fiber. Pump field $\hat{a}_0$, signal field $\hat{a}_1$, and idle field $\hat{a}_2$ are interactive in the cavity. χ is the nonlinear coefficient. The TMSS ($\hat{a}_{1(2)}^{\text{out}}$) is generated from single NOPA and then distributed to quantum users ($\hat{b}_{1(2)}$).

The schematic of the remote distribution scheme of quantum coherence resources through optical fibers is shown in Fig. 1. The TMSS ($\hat{a}_{1(2)}^{\text{out}}$) is generated from a single NOPA and then distributed to quantum users ($\hat{b}_{1(2)}$) through optical fibers. The pump field ($\hat{a}_0^{\text{in}}$) at the harmonic-wave frequency and a weak signal (ideal) beam ($\hat{a}_{1(2)}^{\text{in}}$) at the subharmonic wave frequency are coupled into the NOPA [49]. The pump mode $\hat{a}_0$, signal mode $\hat{a}_1$, and idle mode $\hat{a}_2$ are interactive in the cavity.

The quantum Langevin motion equations of the intracavity pump field ($\hat{a}_0$) and the signal (ideal) beam ($\hat{a}_{1(2)}$) when the NOPA is operated at the parametric deamplification are given by [50]

$$\tau \frac{d\hat{a}_0(t)}{dt} = \chi \hat{a}_1(t)\hat{a}_2(t) - \gamma_{30}\hat{a}_0(t) + \sqrt{2\gamma_{10}}\hat{a}_0^{\text{in}}(t)$$
$$+ \sqrt{2\gamma_{20}}\hat{c}_0^{\text{in}}(t),$$

$$\tau \frac{d\hat{a}_1(t)}{dt} = -\chi \hat{a}_0(t)\hat{a}_2^\dagger(t) - \gamma_3\hat{a}_1(t) + \sqrt{2\gamma_1}\hat{a}_1^{\text{in}}(t)$$
$$+ \sqrt{2\gamma_2}\hat{c}_1^{\text{in}}(t), \qquad (3)$$

$$\tau \frac{d\hat{a}_2(t)}{dt} = -\chi \hat{a}_0(t)\hat{a}_1^\dagger(t) - \gamma_3\hat{a}_2(t) + \sqrt{2\gamma_1}\hat{a}_2^{\text{in}}(t)$$
$$+ \sqrt{2\gamma_2}\hat{c}_2^{\text{in}}(t),$$

where τ is the round trip time of light in the NOPA and χ is the parametric coupling constant of the crystal. The transmissivity efficiency of the output coupler of the NOPA for the pump field and the subharmonic optical field are expressed by γ_{10} and γ_1, respectively. All the unwanted other losses ($\hat{c}_i^{\text{in}}$) in NOPA can be thought of as the intracavity losses of the pump field (γ_{20}) and the signal (idler) mode (γ_2), respectively. The total loss of the pump field and signal (ideal) fields for NOPA are $\gamma_{30} = \gamma_{10} + \gamma_{20}$ and $\gamma_3 = \gamma_1 + \gamma_2$, respectively. In the linearized description of fields, the operators can be expressed by the sum of an average steady-state value $\langle \hat{x}_i \rangle (\langle \hat{y}_i \rangle)$ and a fluctuating component $\delta \hat{x}_i (\delta \hat{y}_i)$, that is, $\hat{x}_i = \langle \hat{x}_i \rangle + \delta \hat{x}_i$ ($\hat{y}_i = \langle \hat{y}_i \rangle + \delta \hat{y}_i$). The output and the intracavity optical fields satisfy the following boundary condition: $\hat{a}_i^{\text{out}} = \sqrt{2\gamma_1}\hat{a}_i - \hat{a}_i^{\text{in}}$.

From the fluctuating component motion equation and the relationship between the input and output fields of the NOPA system, the quadrature correlation variances of the output optical fields ($\hat{a}_{1(2)}^{\text{out}}$) can be calculated as

$$\delta\hat{x}_{a1}^{\text{out}} = \frac{-\left(2\gamma_1\delta\hat{x}_{a1}^{\text{in}} + 2\sqrt{\gamma_1\gamma_2}\delta\hat{x}_{c1}^{\text{in}}\right)(\gamma_3 + i\omega\tau) + 2k\gamma_1\delta\hat{x}_{a2}^{\text{in}} + 2k\sqrt{\gamma_1\gamma_2}\delta\hat{x}_{c2}^{\text{in}}}{k^2 - (\gamma_3 + i\omega\tau)^2} - \delta\hat{x}_{a1}^{\text{in}},$$

$$\delta\hat{x}_{a2}^{\text{out}} = \frac{2k\gamma_1\delta\hat{x}_{a1}^{\text{in}} + 2k\sqrt{\gamma_1\gamma_2}\delta\hat{x}_{c1}^{\text{in}} - \left(2\gamma_1\delta\hat{x}_{a2}^{\text{in}} + 2\sqrt{\gamma_1\gamma_2}\delta\hat{x}_{c2}^{\text{in}}\right)(\gamma_3 + i\omega\tau)}{k^2 - (\gamma_3 + i\omega\tau)^2} - \delta\hat{x}_{a2}^{\text{in}},$$

$$\delta\hat{y}_{a1}^{\text{out}} = \frac{-\left(2\gamma_1\delta\hat{y}_{a1}^{\text{in}} + 2\sqrt{\gamma_1\gamma_2}\delta\hat{y}_{c1}^{\text{in}}\right)(\gamma_3 + i\omega\tau) + 2k\gamma_1\delta\hat{y}_{a2}^{\text{in}} + 2k\sqrt{\gamma_1\gamma_2}\delta\hat{y}_{c2}^{\text{in}}}{k^2 - (\gamma_3 + i\omega\tau)^2} - \delta\hat{y}_{a1}^{\text{in}},$$

$$\delta\hat{y}_{a2}^{\text{out}} = \frac{2k\gamma_1\delta\hat{y}_{a1}^{\text{in}} + 2k\sqrt{\gamma_1\gamma_2}\delta\hat{y}_{c1}^{\text{in}} - \left(2\gamma_1\delta\hat{y}_{a2}^{\text{in}} + 2\sqrt{\gamma_1\gamma_2}\delta\hat{y}_{c2}^{\text{in}}\right)(\gamma_3 + i\omega\tau)}{k^2 - (\gamma_3 + i\omega\tau)^2} - \delta\hat{y}_{a2}^{\text{in}}, \tag{4}$$

where $\hat{x}_{a1}^{\text{in}}$, $\hat{y}_{a1}^{\text{in}}$, $\hat{x}_{a2}^{\text{in}}$, $\hat{y}_{a2}^{\text{in}}$, $\hat{x}_{c1}^{\text{in}}$, $\hat{y}_{c1}^{\text{in}}$, $\hat{x}_{c2}^{\text{in}}$, $\hat{y}_{c2}^{\text{in}}$ are the quadrature amplitude and phase operators of the optical modes $\hat{a}_1^{\text{in}}$, $\hat{a}_2^{\text{in}}$, $\hat{c}_1^{\text{in}}$, $\hat{c}_2^{\text{in}}$. ω is the analysis frequency and the nonlinear coupling efficiency k is related to the parametric coupling constant χ and the pump power [51]. Solving the quantum Langevin motion equations and using the input-output relations of the NOPA, the correlation variances of the output optical fields are obtained [52]

$$\langle\delta^2(\hat{x}_{a1}^{\text{out}} + \hat{x}_{a2}^{\text{out}})\rangle = \langle\delta^2(\hat{y}_{a1}^{\text{out}} - \hat{y}_{a2}^{\text{out}})\rangle$$

$$= 2\left[1 - \frac{4k\gamma_1}{(k + \gamma_1 + \gamma_2)^2 + \omega^2\tau^2}\right]$$

$$= 2\left[1 - \frac{4\beta\rho}{(1 + \beta)^2 + \Omega^2}\right], \tag{5}$$

where $\beta = \sqrt{p_{\text{pump}}/p_{\text{th}}} = k/\gamma_3$ is the normalized pump parameter (p_{pump} is the pump power and $p_{\text{th}} = \frac{\gamma_3^2\gamma_{30}^2}{2\gamma_{10}\chi}$ is the threshold pump power of NOPA); $\rho = \gamma_1/\gamma_3$ is the escape efficiency of the NOPA; $\Omega = \omega\tau/\gamma_3$ is the normalized analysis frequency.

Since the displacement $\bar{x}$ of the generated TMSS is zero, the TMSS can be completely represented by its covariance matrix σ. The diagonal elements of the covariance matrix are the variances of the amplitude ($\delta^2\hat{x}_i$) and phase quadratures ($\delta^2\hat{y}_i$) and the nondiagonal elements are the covariances of the amplitude or phase quadratures, which can be calculated by $\sigma_{ij} = 1/2[\delta^2(\mathbf{x}_i + \mathbf{x}_j) - \delta^2\mathbf{x}_i - \delta^2\mathbf{x}_j]$. The covariance matrix of the generated TMSS from the NOPA system is calculated as

$$\sigma = \begin{pmatrix} \mathbf{A} & \mathbf{C} \\ \mathbf{C}^t & \mathbf{B} \end{pmatrix}, \tag{6}$$

where $\mathbf{A} = a\mathbf{I}$ ($\mathbf{B} = b\mathbf{I}$) represents the reduced covariance matrice of the individual submode, $\mathbf{C} = c\mathbf{Z}$ expresses the correlation between the submodes, $\mathbf{I}$ and $\mathbf{Z}$ are Pauli matrices: $\mathbf{I} = \text{Diag}(1, 1)$, $\mathbf{Z} = \text{Diag}(1, -1)$, $a = b = 1 + 2k\gamma_1(m - n)$, $c = -2k\gamma_1(m + n)$, and $m = 1/[\omega^2\tau^2 + (-k + \gamma_1 + \gamma_2)^2]$, $n = 1/[\omega^2\tau^2 + (k + \gamma_1 + \gamma_2)^2]$. The symplectic eigenvalues of the covariance matrix in the standard form can be determined by [53] $\nu_\pm = [\sqrt{\Delta} \pm (b - a)]/2$, where $\Delta = (a + b)^2 - 4c^2$. The positive partial transposition (PPT) criterion [54] is applied to describe the entanglement of the entangled state, which is a sufficient and necessary condition for a two-mode entangled state with continuous variables. The PPT value means the associated smallest symplectic eigenvalue of the partial transpose and it can be determined by $[(\Gamma - \sqrt{\Gamma^2 - 4\det\sigma})/2]^{1/2}$, where $\Gamma = \det\mathbf{A} + \det\mathbf{B} - 2\det\mathbf{C}$. If the smallest symplectic eigenvalue ν is below 1, the state is entangled. Furthermore, smaller ν represents stronger entanglement.

The influence of various parameters of NOPA on the quantum coherence and entanglement of the deterministic generated TMSS is analyzed in detail as shown in Fig. 2. Figure 2(a) is the dependence of quantum coherence and PPT value of TMSS on the transmissivity of the output coupler for a given analysis frequency ($\omega = 2$ MHz). The loss of the intracavity γ_2 is 0.002, and the nonlinear coupling efficiency k is 0.1. The black dash-dotted line a is the corresponding shot noise limit (SNL), the blue dashed line b and red solid line c are quantum coherence and the PPT value of TMSS versus the transmissivity of the NOPA, respectively. The PPT value decreases with the increase of γ_1 when $\gamma_1 < 0.102$, while the PPT value increases with the increase of γ_1 due to the increased vacuum noise introduced when $\gamma_1 > 0.102$. There is a minimum value of the PPT value when $\gamma_1 = 0.102$, which means the highest degree of entanglement. For quantum coherence of TMSS, the best transmissivity is 0.098. The reason for the slight difference between the two optimal transmissivities is the presence of intracavity loss γ_2. The quantum coherence and entanglement of the TMSS can be maximized at $\gamma_1 = 0.1$ if the intracavity loss is reduced to zero.

Figures 2(b) and 2(c) show the calculated dependence of quantum coherence and the PPT value of the output optical fields on the pump parameter β, where the blue dashed line a for $\gamma_1 = 0.1$, $\gamma_2 = 0.001$, the red solid line b for $\gamma_1 = 0.05$, $\gamma_2 = 0.001$, and the green dotted line c for $\gamma_1 = 0.1$, $\gamma_2 = 0.01$, respectively. Trace d is the boundary of the entangled and separable states. The quantum coherence and entanglement of TMSS increases with the increase of the pump parameter β. Comparing traces a and c, it is obvious that the quantum coherence and the entanglement of the output fields is greater when the NOPA with the smaller intracavity loss γ_2 is at a fixed pump parameter. Also, the quantum coherence and entanglement of TMSS can be increased with the increasing output transmissivity efficiency and the decreasing intracavity
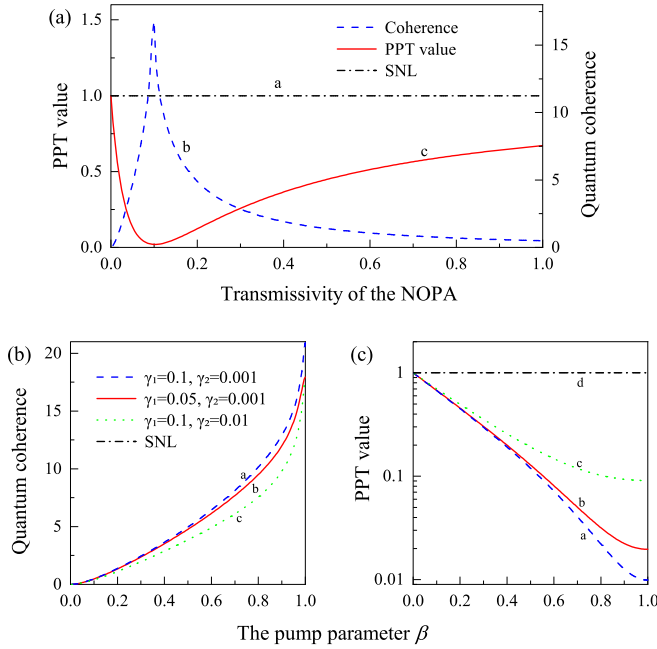
FIG. 2. Dependence of the quantum coherence and entanglement of TMSS on various parameters of NOPA. (a) The quantum coherence and PPT value versus the transmissivity of the output coupler for the subharmonic optical field. Black dash-dotted line "a" is the corresponding SNL, blue dashed line "b," and red solid line "c" are quantum coherence and PPT value of TMSS versus transmissivity of the NOPA, respectively. (b), (c) Dependence of quantum coherence and PPT value of TMSS on the pump parameter, respectively. Blue dashed line a: $\gamma_1 = 0.1$; $\gamma_2 = 0.001$; red solid line b: $\gamma_1 = 0.05$, $\gamma_2 = 0.001$; green dotted line c: $\gamma_1 = 0.1$, $\gamma_2 = 0.01$. Trace d is the boundary of the entangled and separable states. The round trip time τ of light in the cavity is 0.36×10^{-9} s.

loss at a fixed pump parameter. We show that the effects of the pump parameter and intracavity loss on quantum coherence and the entanglement of TMSS are consistent. However, the threshold pump power of the NOPA cavity shows a rising trend with the increase of the output transmissivity efficiency [55]. It is very disadvantageous in terms of the selection of lasers and optical elements in the experiment. Therefore, it is necessary to select the appropriate experimental parameters to improve the quantum coherence and entangled degree of the TMSS.

III. REMOTE DISTRIBUTION OF QUANTUM COHERENCE OF TMSS

The elements of the covariance matrix of the generated TMSS can be given by $a = b = \cosh(2r)$ and $c = -\sinh(2r)$, where r is the squeezing parameter. The TMSS and the local beam are simultaneously transferred in optical fibers to conveniently lock their relative phase, and then quantum users reconstruct the covariance matrix of the distributed optical fields by two sets of balanced homodyne detectors (BHDs) with local (LO) oscillators. When the resulting TMSS propagates in the optical fiber, transmission loss and the excess noise produced by the effect of the depolarized GAWBS is considered. The relationship between the output fields ($\hat{b}_i$) and

input fields ($\hat{a}_i^{\mathrm{out}}$) transmitted in the fiber are given by [56,57]

$$\hat{b}_i = \sqrt{\eta_i}\hat{a}_i^{\mathrm{out}} + \sqrt{1 - \eta_i}\hat{a}_v + \sqrt{\eta_i}\hat{a}_g, \tag{7}$$

where $\hat{a}_g$ is the mode of GAWBS extra noise and $\hat{a}_v$ is the mode of vacuum noise induced by the transmission loss. $\eta_i = \eta_i^c \eta_i^t$ are the total transmission efficiency of TMSS submodes in the optical fibers which consist of the coupling efficiency $\eta_i^c = 0.85$ of the fiber coupler and the fiber transmission efficiency $\eta_i^t = 10^{-\xi l_i/10}$, where ξ is the transmission loss and l_i is the distribution distance. A typical transmission loss of 0.36 dB/km at 1342 nm in the optical fiber is employed in our scheme to quantify the quantum coherence evolution of TMSS. The elements of the covariance matrix of the optical fields over the fiber channels can be expressed as

$$\begin{aligned} a' &= \eta_1 a + 1 - \eta_1 + \eta_1 \varepsilon l_1 I_{\mathrm{LO}}, \\ b' &= \eta_2 b + 1 - \eta_2 + \eta_2 \varepsilon l_2 I_{\mathrm{LO}}, \\ c' &= \sqrt{\eta_1 \eta_2}\, c, \end{aligned} \tag{8}$$

where $\varepsilon l_i I_{\mathrm{LO}}$ is the excess noise induced by the signal beam by the GAWBS processing on $\hat{a}_g$, I_{LO} is the power of the corresponding LO beam before the fiber coupler, and ε is the noise coefficient of GABWS in the fiber.

Here we consider two kinds of realistic scenarios. One is a scenario that the TMSS is distributed to two parties who wish to communicate over two fiber channels, which is referred to as the dual-channel communication scheme ($l_1 = l_2 = l$). Another possibility is that one of the parties holds the quantum-state generator and only one submode needs to propagate through the fiber channel, which is referred to as the single-channel communication scheme ($l_1 = 0, l_2 = l$). In the dual-channel scheme, the experimental data and theoretical prediction of quantum coherence and the PPT value of the distributed TMSS via the distribution distance with different squeezing parameters r are shown in Figs. 3(a) and 3(b), respectively. The power of the LO beam at BHDs after the fibers is 1 mW and ε is 0.16 km^{-1}/ mW^{-1} at the usual analysis frequency range (1.0 MHz to 6.0 MHz). The red solid line a, green dashed line b, and blue dotted line c correspond to the squeezing parameters $r = 0.46, 1, 1.5$, respectively. Trace d is the corresponding SNL. The experimental data at $r = 0.46$ are marked as red circles in the figures [57]. The quantum coherence and entanglement of the distributed TMSS both increase with the increasing squeezing parameter. In addition, the maximum distribution distances of entanglement of TMSS are 2.58 km, 3.45 km, 3.71 km in the dual-channel scheme when the squeezing parameters are 0.46, 1, 1.5, respectively. When the distribution distance is longer than this maximum required value, the entanglement disappears completely between quantum users and the distribution of entanglement cannot be realized. However, the quantum coherence of TMSS still exists even if the entanglement disappears completely. The quantum coherence of TMSS decreases with the enhancement of the transmission loss and the induced GAWBS extra noise in fiber channels, which is because the loss and noise are all incoherent operations and quantum coherence will decrease under incoherent operations [9].

The relationship between entanglement and relative entropy of the distributed TMSS and distribution distance with
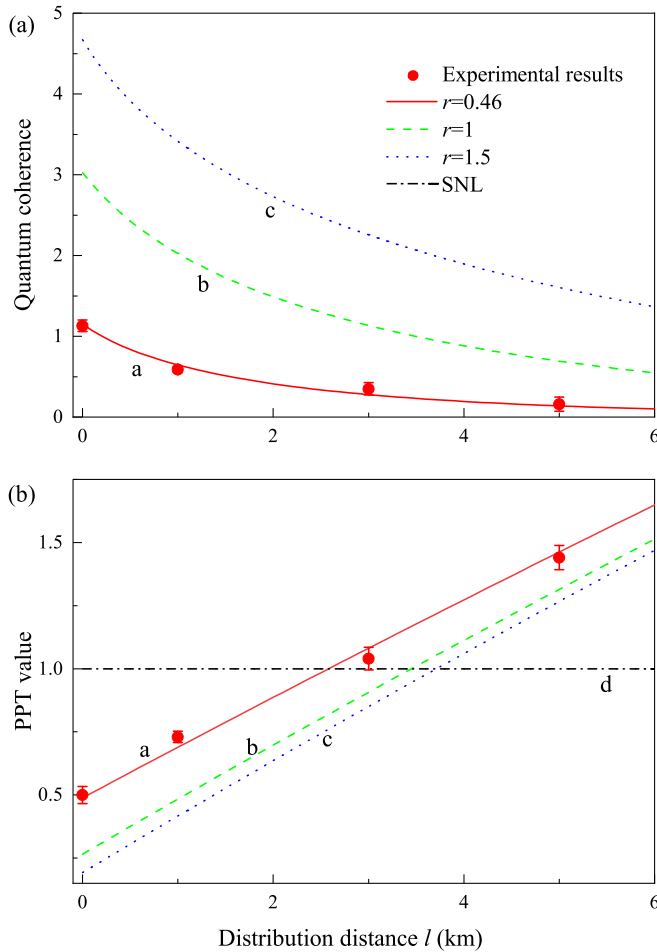
FIG. 3. (a), (b) Quantum coherence and PPT value versus distribution distance with different squeezing parameters. Lines a to c with different styles of curves correspond to squeezing parameter $r = 0.46, 1, 1.5$, respectively. Trace d is the corresponding SNL and the experimental data at $r = 0.46$ are marked as red circles.

FIG. 4. (a), (b) Dependence of quantum coherence and PPT value on distribution distance with the squeezing parameter $r = 0.46$. The traces a to c and traces d to f correspond to the dual-channel scheme and single-channel scheme. Traces a(d), b(e), and c(f) correspond to the power of the LO beam at BHDs is 2 mW, 1 mW, and 0.5 mW, respectively. The black solid line g is the SNL.

different powers of the LO beam after fibers are shown in Figs. 4(a) and 4(b), respectively. The traces a to c and d to f correspond to the dual-channel scheme and single-channel scheme, respectively. The blue dashed line a (blue short dashed line d), red dotted line b (red short dotted line e), and green dash-dotted line c (green short dash-dotted line f) correspond to the power of the LO beam as 2 mW, 1 mW, and 0.5 mW, respectively. The black solid trace g in Fig. 4(b) shows the boundary for entanglement where the PPT value is equal to 1. The experimental data are marked as red circles. The entanglement and quantum coherence of the distribution TMSS both decrease with the increasing power of the LO beam. Comparing traces a and d with the same color, it is obvious that the distribution distance of entanglement in the single-channel scheme is different from the dual-channel communication scheme, and not just double the distance. When the power of the LO beam is 2 mW, 1mW, 0.5 mW, respectively, the maximum distribution distances are 1.42 km (3.86 km), 2.58 km (6.30 km), 4.43 km (9.59 km) in the dual-channel (single-channel) scheme, respectively. Propagation in a single fiber over a certain distance would have a different

effect as the propagation of both submodes in two fibers, over half the distance [58]. The quantum coherence of the TMSS gradually approaches 0 with the increase of distribution distance and it is robust against loss and noise in fiber channels. The physical reason for the robustness of quantum coherence of TMSS in the fiber channel is that the proportion of quantum coherence is decreased when it is mixed with thermal noise, but the quantum coherence disappears completely only when infinite extra noise is involved.

IV. SUMMARY

In summary, we propose a experimentally feasible remote distribution scheme of quantum coherence resources through optical fibers. The generated TMSS from a single NOPA is distributed through fiber channels, and quantum coherence of TMSS is quantified by the relative entropy of the covariance matrix. The evolution of quantum coherence of TMSS in the actual experimental generation system and fiber channels are analyzed in detail. Quantum coherence is robust against loss and extra noise induced by the GAWBS in fiber channels

even if the entanglement disappears completely. The presented research provides the direct reference of experimental research and the foundation of the practical application of quantum coherence in the practical quantum communication network.

ACKNOWLEDGMENTS

[1] P. Skrzypczyk, A. Short, and S. Popescu, Nat. Commun. **5**, 4185 (2014).

[2] M. Lostaglio, D. Jennings, and T. Rudolph, Nat. Commun. **6**, 6383 (2015).

[3] H. L. Shi, S. Ding, Q. K. Wan, X. H. Wang, and W. L. Yang, Phys. Rev. Lett. **129**, 130602 (2022).

[4] C. Li, N. Lambert, Y. Chen, G. Chen, and F. Nori, Sci. Rep. **2**, 885 (2012).

[5] S. Huelga and M. Plenio, Contemp. Phys. **54**, 181 (2013).

[6] M. Hillery, Phys. Rev. A **93**, 012111 (2016).

[7] V. Giovannetti, S. Lloyd, and L. Maccone, Nat. Photonics **5**, 222 (2011).

[8] P. Giorda and M. Allegra, J. Phys. A: Math. Theor. **51**, 025302 (2018).

[9] T. Baumgratz, M. Cramer, and M. B. Plenio, Phys. Rev. Lett. **113**, 140401 (2014).

[10] Y. R. Zhang, L. H. Shao, Y. Li, and H. Fan, Phys. Rev. A **93**, 012334 (2016).

[11] B. Yadin, J. Ma, D. Girolami, M. Gu, and V. Vedral, Phys. Rev. X **6**, 041028 (2016).

[12] C. Yu, Phys. Rev. A **95**, 042337 (2017).

[13] X. Feng and L. Wei, Sci. Rep. **7**, 15492 (2017).

[14] J. Xu, Phys. Rev. A **93**, 032111 (2016).

[15] F. Albarelli, M. G. Genoni, and M. G. A. Paris, Phys. Rev. A **96**, 012337 (2017).

[16] K. D. Wu, Z. Hou, Y. Y. Zhao, G. Y. Xiang, C. F. Li, G. C. Guo, J. Ma, Q. Y. He, J. Thompson, and M. Gu, Phys. Rev. Lett. **121**, 050401 (2018).

[17] Y. Yuan, Z. Hou, Y. Zhao, H. Zhong, G. Xiang, C. Li, and G. Guo, npj Quantum Inf. **6**, 46 (2020).

[18] K. Wu, T. Theurer, G. Xiang, C. Li, G. Guo, M. Plenio, and A. Streltsov, npj Quantum Inf. **6**, 22 (2020).

[19] C. Zhang, T. R. Bromley, Y. F. Huang, H. Cao, W. M. Lv, B. H. Liu, C. F. Li, G. C. Guo, M. Cianciaruso, and G. Adesso, Phys. Rev. Lett. **123**, 180504 (2019).

[20] H. Xu, F. Xu, T. Theurer, D. Egloff, Z. W. Liu, N. Yu, M. B. Plenio, and L. Zhang, Phys. Rev. Lett. **125**, 060404 (2020).

[21] S. Designolle, R. Uola, K. Luoma, and N. Brunner, Phys. Rev. Lett. **126**, 220404 (2021).

[22] R. Takagi and N. Shiraishi, Phys. Rev. Lett. **128**, 240501 (2022).

[23] C. Lüders, M. Pukrop, F. Barkhausen, E. Rozas, C. Schneider, S. Höfling, J. Sperling, S. Schumacher, and M. Aßmann, Phys. Rev. Lett. **130**, 113601 (2023).

[24] Z. Ma, J. Cui, Z. Cao, S. Fei, V. Vedral, T. Byrnesand, and C. Radhakrishnan, Europhys. Lett. **125**, 50005 (2019).

[25] H. Cao, C. Radhakrishnan, M. Su, M. M. Ali, C. Zhang, Y. F. Huang, T. Byrnes, C. F. Li, and G. C. Guo, Phys. Rev. A **102**, 012403 (2020).

[26] H. Kang, D. Han, N. Wang, Y. Liu, S. Hao, and X. Su, Photon. Res. **9**, 1330 (2021).

[27] M. Zhang, H. Kang, M. Wang, F. Xu, X. Su, and K. Peng, Photon. Res. **9**, 887 (2021).

[28] U. L. Andersen, J. S. Neergaard-Nielsen, P. van Loock, and A. Furusawa, Nat. Phys. **11**, 713 (2015).

[29] H. J. Kimble, Nature (London) **453**, 1023 (2008).

[30] C. Peuntinger, B. Heim, C. R. Müller, C. Gabriel, C. Marquardt, and G. Leuchs, Phys. Rev. Lett. **113**, 060502 (2014).

[31] Y. Zhou, J. Yu, Z. Yan, X. Jia, J. Zhang, C. Xie, and K. Peng, Phys. Rev. Lett. **121**, 150502 (2018).

[32] Z. Yan, L. Wu, X. Jia, Y. Liu, R. Deng, S. Li, H. Wang, C. Xie, and K. Peng, Nat. Commun. **8**, 718 (2017).

[33] W. Wang, K. Zhang, and J. Jing, Phys. Rev. Lett. **125**, 140501 (2020).

[34] L. Wu, T. Chai, Y. Liu, Y. Zhou, J. Qin, Z. Yan, and X. Jia, Opt. Express **30**, 6388 (2022).

[35] J. Ren, P. Xu, H. Yong, L. Zhang, S. Liao, J. Yin, W. Liu, W. Cai, M. Yang, L. Li *et al.*, Nature (London) **549**, 70 (2017).

[36] S. Liao, W. Cai, and W. Liu, Nature (London) **549**, 43 (2017).

[37] X. Jia, Z. Yan, Z. Duan, X. Su, H. Wang, C. Xie, and K. Peng, Phys. Rev. Lett. **109**, 253604 (2012).

[38] M. Huo, J. Qin, Z. Yan, Z. Qin, X. Su, X. Jia, C. Xie, and K. Peng, Sci. Adv. **4**, eaas9401 (2018).

[39] J. Feng, Z. Wan, Y. Li, and K. Zhang, Opt. Lett. **42**, 3399 (2017).

[40] F. Hou, R. Quan, R. Dong, X. Xiang, B. Li, T. Liu, X. Yang, H. Li, L. You, Z. Wang, and S. Zhang, Phys. Rev. A **100**, 023849 (2019).

[41] Z. Yan, J. Qin, Z. Qin, X. Su, X. Jia, C. Xie, and K. Peng, Fundam. Res. **1**, 43 (2021).

[42] Y. Tian, P. Wang, J. Liu, S. Du, W. Liu, Z. Lu, X. Wang, and Y. Li, Optica **9**, 492 (2022).

[43] D. Huang, P. Huang, D. Lin, and G. Zeng, Sci. Rep. **6**, 19201 (2016).

[44] H.-L. Yin, T.-Y. Chen, Z.-W. Yu, H. Liu, L.-X. You, Y.-H. Zhou, S.-J. Chen, Y. Mao, M.-Q. Huang, W.-J. Zhang, H. Chen, M. J. Li, D. Nolan, F. Zhou, X. Jiang, Z. Wang, Q. Zhang, X.-B. Wang, and J.-W. Pan, Measurement-Device-Independent Quantum Key Distribution Over a 404 km Optical Fiber, Phys. Rev. Lett. **117**, 190501 (2016).

[45] Y. Zhang, Z. Chen, S. Pirandola, X. Wang, C. Zhou, B. Chu, Y. Zhao, B. Xu, S. Yu, and H. Guo, Phys. Rev. Lett. **125**, 010502 (2020).

[46] M. Pittaluga, M. Minder, M. Lucamarini, M. Sanzaro, R. I. Woodward, M. Li, Z. Yuan, and A. J. Shields, Nat. Photonics **15**, 530 (2021).

[47] R. M. Shelby, M. D. Levenson, and P. W. Bayer, Phys. Rev. Lett. **54**, 939 (1985).

[48] X. Wang, T. Hiroshima, A. Tomitam, and M. Hayashi, Phys. Rep. **448**, 1 (2007).

[49] J. Yu, Y. Qin, J. Qin, H. Wang, Z. Yan, X. Jia, and K. Peng, Phys. Rev. Appl. **13**, 024037 (2020).

[50] C. Fabre, E. Giacobino, A. Heidmann, and S. Reynaud, J. Phys. France **50**, 1209 (1989).

[51] H. Chen and J. Zhang, Phys. Rev. A **79**, 063826 (2009).

[52] Z. Yan, X. Jia, X. Su, Z. Duan, C. Xie, and K. Peng, Phys. Rev. A **85**, 040305(R) (2012).

[53] C. Weedbrook, S. Pirandola, R. García-Patrón, N. J. Cerf, T. C. Ralph, J. H. Shapiro, and S. Lloyd, Rev. Mod. Phys. **84**, 621 (2012).

[54] R. Simon, Phys. Rev. Lett. **84**, 2726 (2000).

[55] Y. Zhou, X. Jia, F. Li, J. Yu, C. Xie, and K. Peng, Sci. Rep. **5**, 11132 (2015).

[56] Y. Li, N. Wang, X. Wang, and Z. Bai, J. Opt. Soc. Am. B **31**, 2379 (2014).

[57] J. Qin, J. Cheng, S. Liang, Z. Yan, X. Jia, and K. Peng, Applied Sciences **9**, 2397 (2019).

[58] F. A. S. Barbosa, A. J. Faria, A. S. Coelho, K. N. Cassemiro, A. S. Villar, P. Nussenzveig, and M. Martinelli, Phys. Rev. A **84**, 052330 (2011).